Eur. Phys. J. D **10**, 39–52 (2000)

THE EUROPEAN PHYSICAL JOURNAL D

EDP Sciences

Energy loss of 18 keV electrons in gaseous T_2 and quench condensed D_2 films

V.N. Aseev[1], A.I. Belesev[1], A.I. Berlev[1], E.V. Geraskin[1], O.V. Kazachenko[1], Yu.E. Kuznetsov[1], V.M. Lobashev[1], R.P. Ostroumov[1], N.A. Titov[1], S.V. Zadorozhny[1], Yu.I. Zakharov[1], J. Bonn[2], B. Bornschein[2], L. Bornschein[2], E.W. Otten[2], M. Przyrembel[2], Ch. Weinheimer[2,a], and A. Saenz[3,b]

[1] Institute for Nuclear Research, Academy of Sciences of Russia, 60th October Anniversary Prospect 7a, 117312 Moscow, Russia
[2] Institute of Physics, Joh. Gutenberg University, 55099 Mainz, Germany
[3] Max-Planck-Institute for Quantum Optics, Theory Group, 85748 Garching, Germany

Received 24 August 1999

Abstract. Measurements of the energy loss of fast electrons at an energy of 18 keV have been performed on molecules of hydrogen isotopes, gaseous T_2 and frozen D_2. Whereas in the case of gaseous T_2 the values of total inelastic cross-section ($\sigma_{\mathrm{tot,\ gaseous}} = (3.40 \pm 0.07) \times 10^{-18}$ cm^2 for $E = 18.6$ keV), average energy loss ($\overline{\varepsilon}_{\mathrm{gaseous}} = (29.9 \pm 1.0)$ eV) and peak position of the energy loss spectra ($\varepsilon_{1,\ \mathrm{gaseous}} = 12.6$ eV) agree well with the expectations, the corresponding values for quench condensed D_2 differ significantly from the ones for gaseous T_2. We observe a significant lower total inelastic cross-section ($\sigma_{\mathrm{tot,\ solid}} = (2.98 \pm 0.16) \times 10^{-18}$ cm^2, for $E = 18.6$ keV) larger average energy loss ($\overline{\varepsilon}_{\mathrm{solid}} = (34.4 \pm 3.0)$ eV) and higher peak position ($\varepsilon_{1,\ \mathrm{solid}} = (14.1^{+0.7}_{-0.6})$ eV). These differences may be interpreted in terms of changes of the final state spectrum. A CI calculation for a D_2 cluster shows indeed a clear shift of the excited states in agreement with the observation.

PACS. 34.80.Gs Molecular excitation and ionization by electron impact – 78.90.+t Other topics in optical properties, condensed matter spectroscopy and other interactions of particles and radiation with condensed matter

1 Introduction

Interaction of electrons with molecular hydrogen is a classical task of fundamental physics. In spite of significant efforts, a comprehensive solution of this problem has not yet been achieved. In particular, precise knowledge of the total and differential inelastic cross-section of multi keV electrons interacting with molecules of hydrogen isotopes is of great importance for astrophysics, plasmaphysics and some domains of nuclear physics. In this paper we report on measurements of the inelastic cross-section of electrons scattered at an energy of around 18 keV from molecular tritium and deuterium in gaseous and solid state, respectively. These data are of crucial importance for a precision analysis of measurements of the β spectrum of molecular tritium in search for a non zero rest mass of the electron antineutrino emitted simultaneously. Apart from this problem they are of self-contained value as stated above.

Besides measurements with low energetic electrons in the eV or few keV range in the past two measurements of the differential inelastic cross-section of energetic (25 keV) electrons on H_2 have been reported, one for small scattering angles $\theta \approx 0.01°$ [1] the other in the range $1° \leq \theta \leq 10°$ [2]. Neither of them covers the full angular range of the inelastic cross-section. Earlier measured energy loss spectra for solid molecular hydrogen gave hints to differ from that in the gaseous phase by a shift of about 1 eV towards higher energy losses [3,4]. Investigations of the photoabsorption of VUV photons in films of solid molecular hydrogen or deuterium [5,6] show significantly different spectra compared to the one in gaseous molecular hydrogen. Although these spectra of solid films are not fully understood they exhibit structures in the 14–20 eV range which have no parentage in the electronic excitations of the isolated molecule.

The two experiments at Troitsk and Mainz presented here have been performed with spectrometers which also served for the precision measurements of the β spectrum from T_2 [7,8]. Both follow the same spectroscopic principle, namely, magnetic adiabatic collimation followed by an electrostatic filter (MAC E filter) which shall be explained here in brief: electrons emerging isotropically with a broad spectrum from some source or target region within a strong magnetic field B_{S} of order 1 T are guided along the field lines into a low field $B_{\mathrm{A}} \leq 1$ mT which leads into

[a] e-mail: christian.weinheimer@uni-mainz.de
[b] e-mail: ajs@mpq.mpg.de

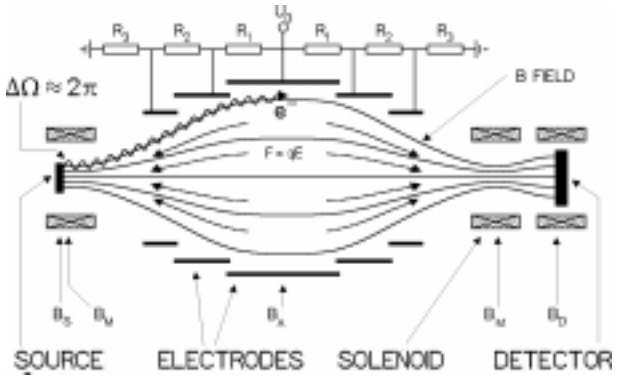

Fig. 1. Principle of a MAC E filter.

an electrostatic analysing potential U (see Fig. 1). Those with a longitudinal energy $E_\parallel \geq qU$ pass the barrier and are collimated magnetically by the field B_D onto a solid state detector. The extraordinary sharpness of the filter stems from the adiabatic transformation of the transverse energy $E_\perp$ of the cyclotron motion into longitudinal energy $E_\parallel$ along the field lines on the way into the B_A region. Only $E_\parallel$ is analysed by the electrostatic potential. A magnetic mirror (pinch) between source and analysing region with a field $B_\mathrm{M} > B_\mathrm{S}$ limits the solid angle accepted from the source or target region to a maximum polar angle

$$\vartheta_{\mathrm{S,max}} = \arcsin(\sqrt{B_\mathrm{S}/B_\mathrm{M}}). \tag{1}$$

The transmission function of the filter for monoenergetic electrons with starting angle $\theta < \vartheta_{\mathrm{S,max}}$ from an isotropic source of energy E rises from zero to one within a relative energy interval ΔE with

$$\Delta E/E = B_\mathrm{A}/B_\mathrm{M}. \tag{2}$$

It is given as a function of U by

$$T(E, qU) = \begin{cases} 0, & E - qU < 0 \\ \dfrac{\left(1 - \sqrt{1 - \dfrac{E - qU}{E}\dfrac{B_\mathrm{S}}{B_\mathrm{A}}}\right)}{\left(1 - \sqrt{1 - \dfrac{\Delta E}{E}\dfrac{B_\mathrm{S}}{B_\mathrm{A}}}\right)}, & 0 \leq E - qU \leq \Delta E \\ 1, & E - qU > \Delta E. \end{cases} \tag{3}$$

Hence, the signal rate R is the integral of the transmitted part of the spectrum S

$$R(qU) = \int_{qU}^{\infty} S(E)T(E, qU)\mathrm{d}E. \tag{4}$$

The main difference between the two set-ups regards the T_2 source: Troitsk is using a long tube with gaseous T_2, whereas Mainz has chosen a solid T_2 film, quench-condensed on a graphite substrate. In spite of the weak molecular van der Waals potential between hydrogen molecules, this difference in phase may be accompanied by some change of the energy loss spectrum of traversing electrons. Therefore, it has to be measured in both phases separately. In Sections 2 and 3 we describe the measurements of the energy loss spectrum of fast electrons in the gaseous phase at Troitsk and in the solid phase at Mainz, respectively. Section 4 deals with a theoretical calculation, performed at MPQ (Garching), treating the difference between the energy loss spectra in gaseous and solid T_2.

2 Study of inelastic scattering of electrons from gaseous tritium

2.1 Experimental set-up

The objective of this experiment is a measurement of the integral spectrum of energy losses for 18.6 keV electrons passing a gaseous T_2 target. As mentioned above it has been carried out at the "Troitsk ν mass set-up" which represents an integral electrostatic spectrometer with adiabatic magnetic collimation and a windowless gaseous T_2 source [7]. The field maximum B_M in the pinch is in the range of 6 T to 8 T, the field minimum B_A in the analysing region is chosen between 1.2 mT and 1.6 mT, providing an energy filter width $\Delta E = 3.5$ eV at the given electron energy. The fields are produced by superconducting solenoids. Particular coils shape the field transition into the analysing region of the filter. A cylindrical electrode in the center provides an analysing potential U with a constant top ($\Delta U/U \leq 2 \times 10^{-5}$) over the full cross-section of its analysing plane.

To the side of the source the strong pinch field transforms smoothly into the weaker field 4–5 T *via* several bents which allow to block the T_2 gas from the spectrometer by differential pumping and LHe-cooled cryotraps. The main part of the T_2 gas is contained in a 3 m long tube cooled down to 27 K in the field $B_\mathrm{S} = 0.8$ T. The gas is fed into the center of the tube and pumped out at both ends through narrower tubes, 0.8 m long and reduced by a factor of 6 in cross-section. Consequently, the field has to be raised there by the same factor up to 5 T in order to still contain the same magnetic flux tube as the wider central section. Note, that the electrons are finally guided within this flux tube from the source to the detector. The T_2 density decreases linearly along these differential pumping tubes by a factor of roughly 100. The T_2 gas is recycled to the inlet after recompression and purification.

All the magnetic and electric fields of the set-up are adjusted to preserve adiabaticity of electron motion. The detector thus counts only electrons moving inside that sector of the magnetic flux tube which crosses the detector area. The flux tube is adjusted as not to touch any walls in the source (besides its rear part, obviously) nor in the spectrometer, and it provides (besides the broadening due to the cyclotron radius) a strict point to point image from the rear of the source to the detector. From this magnetic optics one derives the luminosity of the spectrometer,

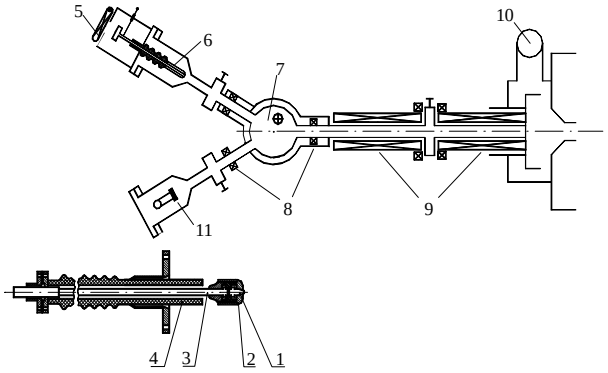

Fig. 2. Monochromatic electron source of Troitsk setup. 1: Quartz tip with gold film, 2: nose of the electrode, 3: tube lightguide, 4: insulator, 5: ultraviolet lamp, 6: electron gun, 7: deflection magnet, 8: focusing short solenoids, 9: solenoids of the transport channel, 10: mercury diffusion pump, 11: monitor detector.

defined as the cross-section of the source A_S times the solid angle of the analysed particle beam to be

$$L = A_S(1 - \cos\vartheta_{S,max})/2 = A_S(1 - \sqrt{1 - B_S/B_M})/2. \quad (5)$$

In order to measure the energy loss spectrum in the T_2 gas, a monochromatic electron beam is fed from the rear into the T_2 source *via* a 1 m long and 1 cm wide transport channel, kept in a guiding field of only 30 mT. The adiabatic transition into the much higher source field blows up the solid angle of the injected electron beam to more then 2π (*i.e.*, the major part of the beam is reflected). Therefore the angular distribution of the beam inside the T_2 target is almost isotropic with an accuracy of about 20%. This facilitates the calculation of the average path length of the electrons spiralling through the target. The electron gun is at 18 kV to 19 kV negative potential. Electrons are emitted by photo effect from a thin, transparent gold film (30 μg/cm^2) on a quartz window placed at the tip of the cathode (see Fig. 2). It is illuminated from the rear with ultraviolet light through a light pipe. The emittance of the gun is determined by the size and curvature of the cathode tip. It has been chosen such as not to touch the walls of the transport channel to the source which is the narrowest part in the whole beam optics considering its low guiding field. Thus, the electron beam does not suffer any scattering besides from the tritium gas.

Focusing of the electron beam onto the entrance of the transport channel is provided by two short solenoids with a 30° bent provided by a transverse magnetic field in between. A diffusion pump at the place of the deflection magnet (7 in Fig. 2) provides a further suppression of tritium pressure by a factor of 100 with respect to the first pumping port at the end of the source. Previously, the electron gun was placed right there at a pressure of around 2×10^{-5} torr. It caused a large contamination by electrons emitted from the cathode by ion bombardment. These electrons had a much larger energy spread of about 10 eV and occurred frequently as multi-electron events. In the present configuration this fraction is decreased to the percent level. Moreover, the deflection magnet prevents electrons from being temporarily trapped between the tip of the cathode and the magnetic pinch. This effect provoked multiple passage of electrons through the target before passing the pinch and thus distorted the energy spectrum. With reversed field this magnet is used in addition to deflect β particles emerging from the T_2 source onto a detector in the second arm of the deflection unit (see Fig. 2). In this mode it serves for monitoring the source intensity in the course of measuring the β spectrum.

The energy spread of photo electrons emitted from the gun is given by the difference $E_\gamma - W$, where E_γ is the effective short wave length limit of the photons set by the spectra of lamp emission and window transmission, respectively. W is the work function of gold (4.3 eV). In addition, the emission spectrum is softened by relaxation of the photo electrons within the gold film. Combining both spectral factors, one estimates an effective emission width of the gun of 0.5 eV for a mercury lamp and 0.7 eV for a deuterium lamp. The latter was preferred in all measurements for its better stability.

2.2 Measurements and analysis of the data

Measurements of the transmission spectrum of electrons through the T_2 source were performed with fixed initial electron energy E well above the endpoint of the tritium β spectrum at $E_0 = 18.570$ keV. The spectrometer potential was scanned from a value slightly above the gun potential into the tritium β spectrum down to 18.4 keV. At each voltage step the signal was measured for 5 to 10 s. The direction of scanning was changed periodically. The following measuring modes were performed sequentially:

mode 1: N_1 counts collected with tritium in the source and the deuterium lamp on;
mode 2: N_2 counts collected with tritium and lamp off;
mode 3: N_3 counts collected without tritium and lamp on;
mode 4: N_4 counts collected without tritium and lamp off.

The count rate of electrons from the electron gun was close to 8 kHz. After each set of these 4 scans, the transport channel was closed by a valve and the β count rate in a reference point at 18.0 keV was measured as well as the mass spectrum of the source. All data were corrected for dead time (4%). This procedure was repeated 6 to 8 times. Then the measurements were repeated at a different density and tritium content of the source. The difference spectrum $N_1 - N_2$ represents the integral spectrum of electrons emitted by the gun and transmitted through the tritium target as function of the filter potential U. The difference $N_3 - N_4$ serves for normalising the electron beam intensity at empty source corrected for background. The slope of this spectrum at the transmission point was used as an experimental resolution function, being a convolution of the spectrometer resolution function (3), with the energy

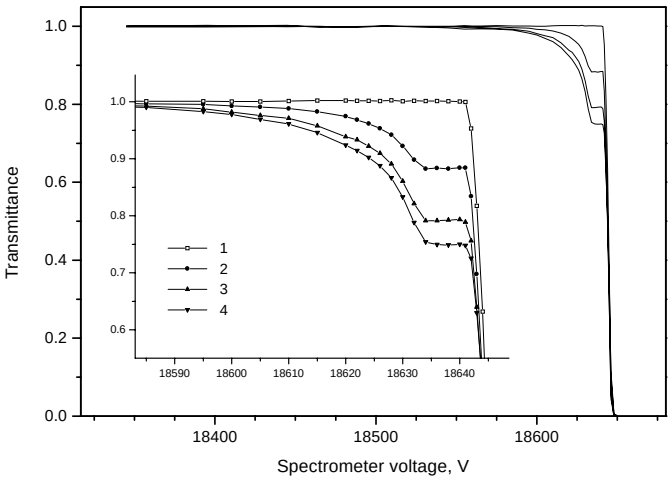

Fig. 3. Electron transmission spectra measured with Troitsk setup. 1: Transmission spectrum without tritium, 2–4: spectra at various density and tritium percentage.

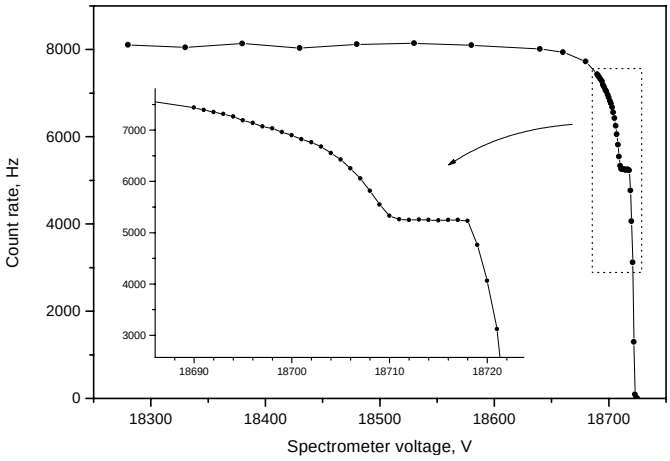

Fig. 4. Integral electron transmission spectrum measured with Troitsk setup with finer point density compared to Figure 3.

and angular distribution of the gun. The spectra of integral energy losses are shown in Figures 3 and 4. All curves show very clearly a distinct shoulder which separates electrons having passed the source without losses from those which underwent inelastic scattering. The no-hit transmission coefficient is determined at the shoulder as

$$K = (N_1 - N_2)/(N_3 - N_4) = \exp(-\mu\sigma_{\rm tot}). \qquad (6)$$

Here $\sigma_{\rm tot}$ is the total inelastic cross-section, $\mu = \rho l$ is the effective column density of the tritium gas, corrected for the spiral roundabout of the electron track through the gas. One thus obtains $\sigma_{\rm tot} = -\ln(K)/\mu$. The precise knowledge of the luminosity L of equation (5) as well as a strict fulfilment of the adiabaticity allows to calculate the average column density of hydrogen isotopes in the tube from a measurement of the β count rate in the reference point and of the isotopic composition of the gas as measured by the mass spectrometer. At that point it should be mentioned that the efficiency of the β detector amounts to practically 100% since electrons which are backscattered

Table 1. Results of total inelastic cross-section measurements of 18.6 keV electrons in gaseous T_2.

	M [s^{-1}]	$T_{\%}$ [%]	$\ln(K)$	$\sigma_{\rm tot}$ [10^{-18} cm^2]
1	347.1±2.1	75.1±1.1	0.126±0.001	3.45±0.09
2	595.2±1.7	67.0±1.0	0.243±0.002	3.35±0.07
3	774.2±1.5	70.7±1.1	0.290±0.02	3.34±0.06
4	808.5±1.7	47.2±1.0	0.438 ±0.07	3.43±0.06
average				3.40±0.07

from its surface with some energy loss are repelled by the electric field back onto the detector until they have lost all of their energy to the detector. The total column density of hydrogen molecules is then given by

$$\mu = M[2C\delta T_{\%} L_{\rm tot}]^{-1}. \qquad (7)$$

Here M is the β count rate at the reference point $qU_{\rm mon} = 18.0$ keV, $C = \ln(2)T_{1/2}^{-1} = 1.79 \times 10^{-9}$ s^{-1} is the decay probability of tritium per unit time, taking into account the final states, $\delta = (35/16)0.84 \sum_i V_i[(E_{0,i} - qU_{\rm mon})/E_{0,i}]^3$ is the ratio of counting rate at reference point ($qU_{\rm mon}$) to total rate in the spectrum, obtained by integration of a classical Fermi spectrum. The sum runs over all final states i of the daughter molecule (T^3He^+), E_{0i} is the β endpoint energy of the ith final state, V_i its population probability. The factor 0.84 stems from the Fermi function. $T_{\%}$ is the isotopic tritium abundance in the source. $L_{\rm tot}$ is the total luminosity (compare Eq. (5)) which is used instead of L in the case of a complex source geometry.

In calculating $L_{\rm tot}$ we have to take into account that a certain fraction of the source strength is contained in the two differential pumping tubes of total length 1.6 m where the field is 5 T as compared to 0.8 T in the 3 m long main source tube. According to equation (5) this fraction contributes with a larger solid angle to the luminosity. Taking into account that the density in the first amounts in average to 0.5 of the maximal value, we thus obtain $L_{\rm tot} = 0.79L_{0.8\rm T} + 0.21L_{5\rm T}$. Corrections for the spiral roundabout of the track of gun electrons through the source were calculated with the same weights and amounted to 1.067. The statistical error was of order 2×10^{-3}. The scatter of data was dominated by fluctuations of the lamp intensity and errors of mass spectrometry (2%). Correction to M due to selfabsorption was introduced in first order approximation and amounted to 1–3%.

Typical results obtained at different values of gas density and tritium content are given in Table 1. For the total inelastic cross-section of 18.6 keV electrons scattered from molecular tritium and integrated up to a maximum energy loss of 200 eV, we obtain the final experimental results of Table 1.

The final result $\sigma_{\rm tot} = (3.40 \pm 0.07) \times 10^{-18}$ cm^2 is in good agreement with the theoretical value of 3.456×10^{-18} cm^2 [9]. The contribution to $\sigma_{\rm tot}$ of scattering events

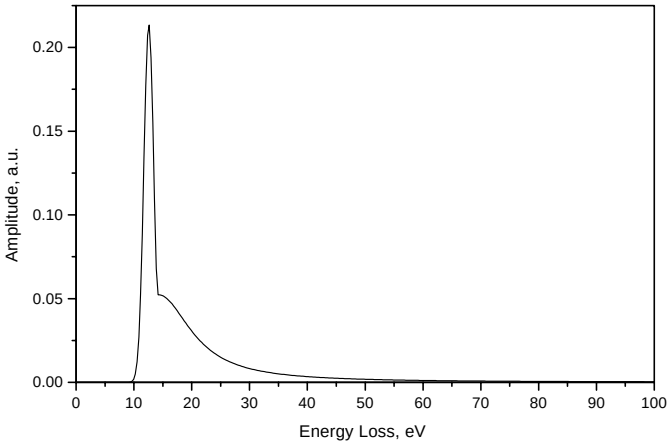

Fig. 5. The fitted energy loss spectrum for single scattering.

with energy losses higher than 200 eV are negligible within present errors.

2.3 The energy loss spectrum

Integral spectra of electrons transmitted through the gaseous target of molecular hydrogen are shown in Figures 3 and 4 as function of the lower integration limit which is the filter potential qU. Differentiation of the spectra would yield directly the original energy loss spectrum as function of the energy loss ε, but meets significant difficulties due to the discontinuity of the derivative at 3 points. Therefore, we were forced to parameterise the shape of the energy loss spectrum, in accordance with the widely adopted practise, and then to fit it to the experimental integral spectrum. In former papers [7,10] the energy loss spectrum had been modelled by two Lorentzians: one for the excitation of bound electronic states up to the ionisation energy of 15.45 eV and the second one for the continuum. Whereas the Lorentzian meets the correct asymptotic ε^{-2} dependence for ionisation, we found that a Gaussian provides a better fit for the excitation spectrum since it allows for a much sharper bent at the excitation threshold (see Fig. 5). Thus the shape of the energy loss spectrum for a single scattering within the target was taken as:

$$f(\varepsilon) = \begin{cases} A_1 \exp\left(-\dfrac{2(\varepsilon-\varepsilon_1)^2}{w_1^2}\right) & \text{for } \varepsilon < \varepsilon_c \\ A_2 \dfrac{w_2^2}{w_2^2 + 4(\varepsilon-\varepsilon_2)^2} & \text{for } \varepsilon \geq \varepsilon_c. \end{cases} \quad (8)$$

The function $f(\varepsilon)$ is normalised and describes the shape of the inelastic cross-section:

$$\int_0^{E/2} f(\varepsilon)\mathrm{d}\varepsilon = 1 \quad (9)$$

$$\frac{\mathrm{d}\sigma}{\mathrm{d}\varepsilon} = \sigma_{\mathrm{tot}} f(\varepsilon). \quad (10)$$

The parameters $A_{1,2}$, $\varepsilon_{1,2}$, $w_{1,2}$ are the fit parameters describing amplitude, central position and width of the Gaussian and Lorentzian, respectively. The matching point ε_c is chosen by the fit in such a way that for the fitted couple of amplitudes A_1 and A_2 both parts of the energy loss function have a smooth connection at $\varepsilon = \varepsilon_c$. The unphysical kink of the model spectrum at the matching point has little effect in practice since it is washed out – like any other spectral fine detail – by convolution with the transmission function (3) (compare also the analysis with other trial functions in Sect. 3.2). Satisfactory fits could be achieved with $\varepsilon_1 = 12.6$ eV within a range of about ± 0.3 eV. Therefore ε_1 was fixed to 12.6 eV for the fits. Note, however, that this fixing suppresses the correlation between the fit parameters and hence of the fit errors by parts.

Finally, we have to include multiple scattering events in the function fitting the signal $R(qU)$ of equation (4) by modifying the transmission function which then reads

$$T'(E,qU) = \int_0^{E/2} T(E-\varepsilon, qU) \times \big(P_0\delta(\varepsilon) + P_1 f(\varepsilon) + P_2 (f \otimes f)(\varepsilon) + \ldots\big)\mathrm{d}\varepsilon. \quad (11)$$

Here P_i is the probability of an electron scattering i times; it is given by a Poisson distribution $P_i = K(\ln K)^i/n!$ with K being the no-hit transmission coefficient[1] of equation (6). The folding symbol $(f \otimes f)(\varepsilon)$ stands for $\int_0^{E/2} f(\varepsilon-\varepsilon')f(\varepsilon')\mathrm{d}\varepsilon'$. Multiple scattering was included up to the 4th order. The fit was performed with the help of the MINUIT program [13]. The input errors of the experimental transmission signal were determined from the fluctuation of individual scattering points from the fitted curve at energy losses above 150 eV where the signal becomes practically flat. Results are presented in Table 2 for the four sets of data, given in Table 1. The corresponding energy loss function is shown in Figure 5.

The ratio of the excitation to the ionisation fraction of the total cross-section proved to be 51/49. This result barely depends on our particular choice of the model functions but can be read more or less directly from the integral spectra of energy losses in Figures 3 and 4, which pass the 50% level just at the ionisation threshold. The result is at variance with the usually adopted value of 40/60, but is in agreement with the measurement of the total ionisation cross-section of 18.6 keV electrons reported in reference [11]. The mean energy loss per inelastic collision has been derived from this measurement to be

$$\overline{\varepsilon} = (29.9 \pm 1.0)\ \mathrm{eV}, \quad (12)$$

which agrees with the expectation of reference [12]. Finally we mention that the fit result of the Lorentzian amplitude meets asymptotically the corresponding inelastic cross-section of quasi free nonrelativistic Møller scattering [14]

$$\frac{\mathrm{d}\sigma}{\mathrm{d}\varepsilon} \approx \frac{\pi e^4}{E\varepsilon^2} \quad (13)$$

quite precisely.

[1] A detailed averaging of all different path lengths turned out to make only a negligible effect.

Table 2. Results of fitting the parameters of the energy loss spectrum in gaseous T_2.

Parameters	1	2	3	4	average
A_1 [1/eV]	0.204±0.001	0.204±0.001	0.204±0.001	0.204±0.001	0.204 ± 0.001
w_1 [eV]	1.87±0.02	1.83±0.04	1.83±0.03	1.78±0.05	1.85 ± 0.02
ε_1 [eV]	12.6	12.6	12.6	12.6	12.6
A_2 [1/eV]	0.0542±0.0005	0.0561±0.0005	0.0561±0.0007	0.0563±0.0005	0.0556 ± 0.0003
w_2 [eV]	11.5±0.5	12.1±0.2	12.8±0.1	12.5±0.1	12.5 ± 0.1
ε_2 [eV]	14.45±0.04	14.34±0.05	14.30±0.03	14.29±0.06	14.30 ± 0.02
χ^2/d.o.f.	18.0/21	22.3/21	20.9/21	34.2/35	

3 Energy loss measurement in quench condensed D_2 films

3.1 Experimental set-up

The energy loss of electrons in solid deuterium was determined using the set-up of the Mainz Neutrino Mass Experiment, an integral electrostatic spectrometer with adiabatic magnetic collimation [15] similar to the Troitsk setup but using a solid T_2 source instead, quench-condensed on a highly oriented pyrolytic graphite substrate [8]. The field maximum B_M in the pinch is 2.2 T, the field minimum B_A in the analysing region is 0.5 mT, providing a filter width of $\Delta E = 4.4$ eV at the given energy according equation (2). The source was placed in a field of $B_S = 1.1$ T, thus limiting the maximum starting angle accepted by the spectrometer to $\vartheta_{S,max} = 45°$. The fields are produced by superconducting solenoids. A system of 27 cylindrical electrodes provides an analysing potential U with a constant top in the center of $\Delta U/U \leq 2 \times 10^{-5}$ over the full cross-section of its analysing plane.

3.2 Measurements and analysis of the data

Due to the presence of the substrate we cannot perform a transmission experiment with an electron gun but have to choose a radioactive source instead, namely K conversion electrons from ^{83m}Kr. The energy of the K32 conversion line ($E_{K32} = 17.82$ keV, with a Lorentzian width of $\Gamma_{K32} = 2.83$ eV (FWHM) [16]) meets the region of interest around the endpoint $E_0 = 18.57$ keV of tritium β decay. The sublimation characteristics of Kr and D_2 allows to prepare in situ a ^{83m}Kr/ D_2 sandwich by quench condensation [17]. The ^{83m}Kr gas is collected from the decay of a ^{83}Rb source [18]. The ^{83m}Kr halflife of 1.83 h allows measurements with reasonable statistics without risking longterm contamination of the apparatus. After purification by a cryotrap the ^{83m}Kr gas was condensed on the 1.8 K cold graphite substrate (HOPG) as sub monolayer with a typical activity of 10 kBq. An absorber layer of D_2 was then quench condensed on top of the krypton. The D_2 coverage μ, *i.e.* the product of the film thickness d and its molecular density ρ, was measured by laser ellipsometry with a resolution of 4–8%. This relatively large uncertainty was mainly due to imperfect flatness of the substrate and reproducibility of the measurement. The ellipsometry showed that our quench condensed D_2 films were not closely packed. The measurement of the optical refraction index gave $n(D_2) = 1.1415 \pm 0.0020$ at $\lambda = 632$ nm, from which a density of $\rho = 2.70 \times 10^{22}/\mathrm{cm}^3$ can be calculated by Clausius Mosotti's law. This value is 11% smaller than expected for a closely packed D_2 crystal ($\rho = 3.02 \times 10^{22}/\mathrm{cm}^3$). The same holds for the T_2 films used in our β decay measurements [8]. The D_2 coverage was varied for the different measurements between 4 and 14 molecules per Å^2, a measurement without D_2 coverage was carried out as reference.

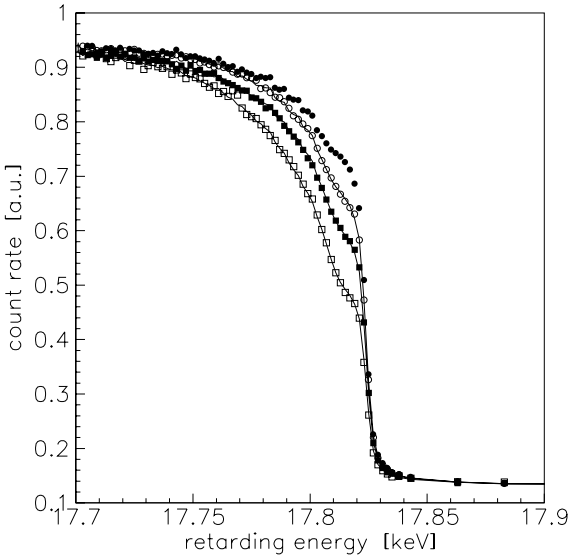

Fig. 6. Mainz integral energy spectra of electrons from a ^{83m}Kr K32 conversion source covered by various D_2 absorbers (see Tab. 3). Open circles: 3.9 Å^{-2}, filled squares: 7.7 Å^{-2}, open squares: 14.3 Å^{-2}, filled circles: no coverage. The lines show fits to the data using the energy loss function given by equation (15). The spectra are normalised to equal K32 conversion line intensity.

Integral energy spectra of transmitted conversion electrons are shown in Figure 6 for the different sandwiches. The K32 conversion line appears as a step at $E = 17.825$ keV. Electrons which have lost energy are shifted towards lower energies. However, the reference spectrum without D_2 coverage already exhibits a complex structure

of low energy satellites due to electron shake on/off in Kr. This drawback inhibits an analytic description of the reference spectrum and hence the deconvolution of the D_2 energy loss function. Therefore, the measured reference spectrum $R(qU)$, which also includes the convolution with the spectrometer transmission function was taken as input for fitting the normalised D_2 energy loss function $f(\varepsilon) = (1/\sigma_{\rm tot})(\mathrm{d}\sigma/\mathrm{d}\varepsilon)$. It describes the shape of a single inelastic scattering process (see Eqs. (9, 10)). The evaluation of the reference spectrum in between measured points was done by linear interpolation. As in Section 2.3 (compare Eq. (11)) multiple scattering was taken into account up to the 3rd order by multiple convolution of $f(\varepsilon)$. This procedure yields the fit function $R'(qU)$, which additionally includes the parameters a and b for normalising the signal and background rates of different runs:

$$R'(qU) = a \int_0^{E/2} R(qU+\varepsilon) \times \big(P_0\delta(\varepsilon) + P_1 f(\varepsilon) + P_2(f\otimes f)(\varepsilon) + \ldots\big)\mathrm{d}\varepsilon \; + b. \quad (14)$$

The multiple scattering probabilities P_i were calculated for a given value of the total inelastic cross-section $\sigma_{\rm tot}$ assuming a Poisson distribution for the scattering processes averaged over all possible paths through the absorber. This average was calculated for a homogeneous D_2 film[2] considering that the electrons were emitted isotropically up to a maximum angle $\vartheta_{\rm S,max}$. While the input parameters μ and $\vartheta_{\rm S,max}$ are known, $\sigma_{\rm tot}$ was fitted to the data. Additional fit parameters were the normalising constants a and b, and an energy shift. This shift compensates small high voltage drifts between measurements as well as a shift of the order of 0.2 eV due to the polarisation energy of the $^{83}Kr^+$ daughter ion due to the coverage with the D_2 film.

For the energy loss function $f(\varepsilon)$ we tried, similar to Section 2.3, different trial functions which consist of a peak representing electronic excitations of D_2, and a smoothly connected tail describing ionisation. As peak functions Gaussians and Lorentzians of various widths were tested, as tail functions truncated Lorentzians and hyperbola of different exponents. These trial functions serve for a phenomenological description of the energy loss function in the relevant region up to energy losses of about 100 eV, to which our measurements were sensitive. Beyond, the integral spectra merge apparently for all D_2 coverages into the uncovered one, telling that $\sigma_{\rm tot}$ is practically exhausted by this interval within the experimental precision (see Fig. 6) To avoid the introduction of a systematic error in the average energy loss $\overline{\varepsilon}$ by using a wrong asymptotic tail, we connected the trial functions for energy losses ε larger than 100 eV to the differential Møller scattering (13). The best agreement between the fit function and the data was obtained by using as trial functions a Gaussian for the peak region combined with a hyperbola of third order for the tail of the energy loss function:

$$f(\varepsilon) = \begin{cases} A\exp\left(-\dfrac{2(\varepsilon-\varepsilon_1)^2}{w_1^2}\right) & \text{for } 0 < \varepsilon < \varepsilon_1 + \Delta\varepsilon_1 \\ A\dfrac{B}{(\varepsilon+\Delta\varepsilon_2)^3} & \text{for } \varepsilon_1+\Delta\varepsilon_1 \le \varepsilon \le 100\ \text{eV} \\ \dfrac{2.4\ \text{eV}}{\varepsilon^2} & \text{for } \varepsilon > 100\ \text{eV}. \end{cases} \quad (15)$$

The amplitude A normalises $f(\varepsilon)$, the factor B is then chosen to provide smooth connection at the matching point $\varepsilon = \varepsilon_1 + \Delta\varepsilon_1$.

Whereas $\sigma_{\rm tot}$ and the calibration parameters of $R'(qU)$ were fitted separately for each data set, the parameters of $f(\varepsilon)$ were determined in a simultaneous fit of all three data sets (χ^2/d.o.f. = 288/298) under the constrained (9). The results of $\sigma_{\rm tot}$ are shown in Table 3. The parameters of $f(\varepsilon)$ were fitted to be

$$A = (0.11^{+0.11}_{-0.03})\ (\text{eV})^{-1}, \quad (16)$$
$$\varepsilon_1 = (14.1^{+0.7}_{-0.6})\ \text{eV}, \quad (17)$$
$$w_1 = (2.5^{+1.5}_{-1.5})\ \text{eV}, \quad (18)$$
$$\Delta\varepsilon_1 = (1.1^{+0.7}_{-0.4})\ \text{eV}, \quad (19)$$
$$\Delta\varepsilon_2 = (2.8^{+1.1}_{-1.1})\ \text{eV}. \quad (20)$$

The individual statistical uncertainties of the parameters (except for the peak position (17) are rather large, but strongly correlated. This result tells on the one hand that the problem of determining the exact shape of $f(\varepsilon)$ by deconvoluting its experimental integral spectrum is not well-posed. On the other hand the strong correlation of these fit parameters is reflected in quite stable values

Table 3. Total inelastic cross-section $\sigma_{\rm tot}$ for the data sets 1–3 obtained for different D_2 coverages μ. The first uncertainty on μ is a purely statistical error, the second one the systematic uncertainty. The first uncertainty of $\sigma_{\rm tot}$ originates from the statistical fit error as well as from the statistical error on μ, the second uncertainty is derived from the systematic uncertainties of the parameters of the trial function as well as of μ. Since the systematic uncertainty on $\sigma_{\rm tot}$ (as well as on μ) is at least partly correlated among the three sets we have averaged its contribution for the final result.

measurement	μ [Å^{-2}]	$\sigma_{\rm tot}$ [10^{-18} cm^2]
1	$3.88 \pm 0.06 \pm 0.33$	$2.94 \pm 0.08 \pm 0.25$
2	$7.73 \pm 0.05 \pm 0.49$	$2.97 \pm 0.04 \pm 0.19$
3	$14.27 \pm 0.05 \pm 0.56$	$3.22 \pm 0.03 \pm 0.13$
average		$3.11 \pm 0.02 \pm 0.17$

[2] We also have investigated the case that the thickness is not completely homogeneous but has some residual roughness due the quench condensation process. Modelling this effect by varying locally the thickness of the D_2 absorber by a Poisson distribution of the number of monolayers does not change the multiple scattering probabilities P_i and the fit results significantly.

of $\sigma_{\rm tot}$ (compare Tab. 3) as well as of the mean energy loss[3]

$$\overline{\varepsilon} = \int_0^{E/2} f(\varepsilon)\varepsilon \mathrm{d}\varepsilon = (34.4 \pm 0.4 \pm 3.0)\ \mathrm{eV}. \qquad (21)$$

That our problem is well-posed with respect to extract the two integral quantities is supported by the fact, that both are stable against exchanging our best trial function (15) by other reasonable trial functions which were mentioned above including the one used in the analysis of scattering from a gaseous target (but with different parameters $A_{1,2}$, $\varepsilon_{1,2}$, $w_{1,2}$ than those of Tab. 2).

The energy loss function $f(\varepsilon)$ derived here can be directly applied to calculate the energy loss of electrons from the endpoint region of tritium β decay within the source [8], the value of $\sigma_{\rm tot}$ has to be slightly rescaled for this purpose from $E_{\rm e} = 17.82$ keV to $E_{\rm e} = 18.6$ keV by a simple $1/E_{\rm e}$ law [9] giving

$$\sigma_{\rm tot}(18.6) = (2.98 \pm 0.02 \pm 0.16) \times 10^{-18}\ \mathrm{cm}^2 \quad (\text{for } E_{\rm e} = 18.6\ \mathrm{keV}). \qquad (22)$$

If we compare the energy loss for gaseous T_2 with the one for quench condensed D_2 we observe two major differences.

1. The peak position ε_1 of $f(\varepsilon)$ for quench condensed D_2 appears at a significantly higher ε value. The shift between the respective values (see Tab. 2 and Eq. (15)) is $1.5^{+0.8}_{-0.7}$ eV. Although for the measurement with quench condensed D_2 the peak position ε_1 and peak width w_1 are not well determined but strongly correlated with each other we can get a reliable value for the shift of the peak position[4] when we compare the peak positions at equal width of $w_1 = 1.85$ eV. Then the peak position for quench condensed D_2 is $\varepsilon_1{}' = 14.0$ eV, the shift compared to Table 2 is still 1.4 eV.
   The shift is also stable when we exchange our best trial function (15) by other reasonable trial functions mentioned above. The values for the shift obtained here are in good agreement with the shifts observed in references [3,4] (compare Tab. 4).
2. The total inelastic cross-section $\sigma_{\rm tot}$ for solid D_2 is found to be $(13 \pm 5)\%$ smaller than for gaseous molecular hydrogen. This difference is also stable against variations of $f(\varepsilon)$ within the given limits.
3. The shift in the peak energy loss is reflected again in the even stronger shift of the mean energy loss per inelastic collision $\Delta\overline{\varepsilon} = (4.5 \pm 3.2)$ eV. The number is less precise than that of the peak shift, but still significant. This shift is only partially due to the shift of the peak. The main contribution comes from a higher fraction of the tail of the energy loss function (see Fig. 7).

[3] The main uncertainty of $\overline{\varepsilon}$ comes from its dependence on the choice of the limit above which the quasielastic Møller scattering was used to describe $f(\varepsilon)$.

[4] A comparison using the energy loss function $f(\varepsilon)$ obtained for gaseous T_2 also for quench condensed D_2 is not possible, since equation (8) using the parameters of Table 2 does not fit our data for quench condensed D_2 even when allowing for a shift of the whole function.

Table 4. Summary of experimental results of energy loss measurements in gaseous T_2 and quench condensed D_2 in comparison with values from literature. The values of the cross-section or stopping power are given for an energy of 18.6 keV.

	gaseous T_2	solid D_2	gaseous H_2
$\sigma_{\rm tot}$ $[10^{-18}\ \mathrm{cm}^2]$	3.40 ± 0.07	2.98 ± 0.16	3.456 [9]
$\overline{\varepsilon}$ [eV]	29.9 ± 1.0	34.4 ± 3.0	
$\sigma_{\rm tot}\overline{\varepsilon}$ $[10^{-18}\ \mathrm{eV\ cm}^2]$	102 ± 4	104 ± 11	104 [12]
ε_1 [eV]	12.6 ± 0.3	$14.1^{+0.7}_{-0.6}$	12.6 [1]

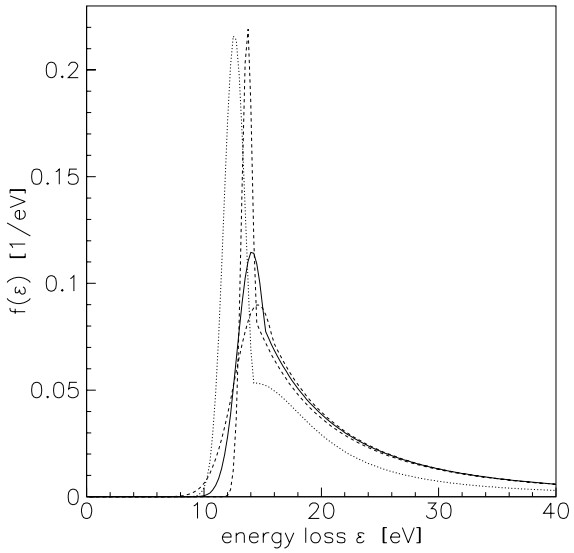

Fig. 7. Normalised energy loss function $f(\varepsilon)$ from fit to Mainz data for quench condensed D_2 absorbers: best fit (solid line), ± 1 standard derivations in line width w_1 (dashed lines). For comparison $f(\varepsilon)$ obtained for gaseous T_2 in Section 2 is plotted also (dotted lines).

The origin of these shifts has to be sought in differences of the final state spectrum of excited electrons which seem to quench part of the energy loss strength. Theoretical grounds of such an effect are discussed in the following section.

4 Solid state effects in quench condensed molecular hydrogen films

4.1 The theoretical model

Solids formed by hydrogen (or its isotopes) possess the rather unique property that a nearly unhindered rotation of the molecules is possible [19]. This is due to the fact that

the molecules in the crystal are bound to each other by long range forces that are comparatively weak and nearly isotropic. This property is accompanied by a rather large intermolecular distance compared to the intramolecular one. As a consequence, the hydrogen molecules in the solid behave very similar to free molecules in gas phase, as is reflected in the rotational spectrum which is nearly identical for the gas and the condensed phase.

On the other hand, photoabsorption studies as well as the present energy loss study indicate a comparatively pronounced change of the spectra when going from the gas phase to the solid. One possible explanation for this observation has been proposed by Ruckman and Moore in [4]. Since the interaction of the ground state wavefunctions between adjacent hydrogen molecules is very small due to the large intermolecular distance, a solid formed by hydrogen molecules (all being in their ground state) behaves nearly as an array of free molecules. However, due to the larger spatial extent of the wavefunction especially of electronically excited hydrogen molecules the (electronic) excitation spectrum will change when going from the gas phase to the solid state. This phenomenon may be understood as a confinement of the excited state wavefunction by the neighbour molecules due to repulsive electrostatic interaction and Pauli blocking. Within this picture the excitation of a molecule within the solid may approximately be viewed as a transition to an excited molecular state that is however confined by the surrounding.

In order to investigate the appropriateness of this model the following approach has been chosen for obtaining a *semi-quantitative* description of the process. Based on a configuration-interaction (CI) method the lowest electronic states of a hydrogen molecule have been investigated. The calculation has been performed for a single (free) molecule and for a molecule surrounded by a cloud of neighbour molecules. A full CI calculation of the complete cluster would however yield the excitation energies of all interacting molecules, and thus it would *e.g.* give different energies for the central molecule than for the outer molecules, since they experience different surroundings due to the finite cluster size. This is correct for a model describing such a cluster, but it is not senseful for the present purpose of modelling the excitation of a single molecule in a solid.

In the present model this problem was avoided in the following way. In a first step the Hartree-Fock orbitals have been evaluated separately for the shell of surrounding molecules and the central molecule. Then a CI calculation of the whole system has been performed in the basis of two-electron configurations formed with the aid of the doubly-filled (closed-shell) Hartree-Fock orbitals of the surrounding and all (occupied and virtual) Hartree-Fock orbitals of the central molecule. In this CI calculation the orbitals of the surrounding molecules were *frozen*, *i.e.* they were left unchanged and their occupation number was fixed. In this way the central molecule is described in a complete way, only limited by the finite basis set used, while the surrounding is described on the level of a static Hartree-Fock approximation. Thus only the modification of the wavefunctions of the central molecule by the surrounding is taken into account, but the polarisation of the surrounding by the central molecule (and its feedback on the wavefunction of the central molecule) is completely neglected.

It may be emphasised that the wavefunctions of the surrounding had been calculated without the central molecule and thus there has been even no polarisation of the surrounding wavefunctions by the ground state wavefunction of the central molecule. The advantage of this fact is that all wavefunctions of the central molecule are treated on the same level of approximation. Finally, it may be noted that due to the static approximation for the surrounding one should expect that the employed model overestimates the confinement effects.

4.2 Computational details

All calculations have been performed with the aid of the quantum-chemistry code GAMESS [20]. This code allows to perform *ab initio* calculations within a basis of Cartesian Gaussians. For describing the surrounding hydrogen molecules a so-called 6-311 G basis set consisting out of 5 s-type Gaussians (where three of them are contracted to one basis function) centered at every hydrogen atom has been used. In the case of the central molecule 10 s-type Gaussians with even-tempered exponents in the range $1398.0a_0^{-2}$ to $0.03a_0^{-2}$ and 9 p-type Gaussians (of p_x, p_y, and p_z type) with even-tempered exponents in the range $400.0a_0^{-2}$ to $0.02a_0^{-2}$ have been placed on every hydrogen atom.

While the Hartree-Fock energy of a single surrounding molecule is of moderate quality (−30.69 eV compared to the Hartree-Fock limit of −30.85 eV, both at the internuclear distance $R = 1.40a_0$), the ground state energy of the central molecule is of good accuracy (−30.84 eV on the Hartree-Fock level and −31.89 eV on the CI level compared to −31.96 eV obtained in the most accurate calculation). The quality of the description of the surrounding molecules could be improved by adding so-called polarisation functions of p-type symmetry (allowing a better description of the chemical bond), but this is computationally very costly (in fact doubling the number of basis functions) and seemed not to be necessary considering the adopted model where the surrounding molecules are not polarised by the central molecule. In the case of the central molecule Gaussians of higher angular momenta would have to be included in order to achieve improved angular correlation and thus energies that are even closer to the best theoretical ones. Again, such improvements were judged to be computationally too expensive regarding the overall simplicity of the model to be worthwhile the efforts.

Since electronic excitations should be fast on the time-scale of nuclear motion, one may assume vertical transitions, *i.e.* transitions at constant internuclear distance. In the present calculations the internuclear distance $R = 1.43a_0$ has been adopted for the central and the surrounding molecules. This value is the average mean

internuclear distance of D_2 and T_2. In order to test the dependence of the results on this parameter, calculations have also been performed using in some cases $R = 1.30$ and $1.50a_0$ for the central molecule.

The geometry of solid hydrogen at low temperatures is rather complicated, since a number of phase transitions has been observed [19]. While for extremely low temperatures a spin-ordered structure has been predicted and observed, solid hydrogen at about 5 K prefers the *hcp* structure. Condensed films or solid hydrogen at temperature around 2 K seem however to form an *fcc* lattice. In the present calculation the *fcc* structure was adopted. Thus the central hydrogen molecule is surrounded by 12 next neighbour molecules. The second coordination shell contains then 6 further molecules. From the density $\rho = 3.02 \times 10^{22}/\mathrm{cm}^3$ (compare Sect. 3.2) one can deduce the unit cell constant $a = 9.65a_0$.

Due to the nearly free rotation of the the H_2 molecules in the solid one has an infinite number of possible orientations of the surrounding molecules to each other and to the central molecule. A complete calculation would require to calculate the spectra for a sufficient number of orientations and to perform an adequate averaging. In the present calculation only three rather extreme cases (with comparatively high ordering) have been considered that all had the advantage of preserving overall C_{4v} symmetry which reduced the computation time.

In the case of the first geometry (cluster I) all molecules are oriented parallel to the same axis. Clusters II and III have been obtained from cluster I by a rotation of the surrounding molecules (keeping the center of mass of each molecule fixed). In cluster II the molecular axis of each surrounding molecule points towards the central molecule, while in cluster III the molecular axis of each surrounding molecule is perpendicular to the line connecting the center of mass of the central molecule with the one of that surrounding molecule. A complete calculation may then *e.g.* be denoted as II'(1.43/9.65). Here II refers to cluster II, the single prime indicates that one shell of surrounding molecules has been included, 1.43 is the internuclear distance of the central molecule (in a_0), and 9.65 is the length a of the cubic unit cell (in a_0).

4.3 Results

Seven electronically excited states (three of them being doubly degenerate Π states) have been considered in this work. They are the energetically lowest lying states obtained with the adopted basis set. In order to allow an estimate of the accuracy of the present calculation (with respect to the treatment of the central molecule), the calculated transition energies with respect to the electronic ground state are compared to literature values in Table 5 for the internuclear distance $R = 1.40a_0$. (An exception is the $H\,^1\Sigma_g^+$ state where only literature values at $R = 1.50a_0$ were available.) The agreement is very satisfactory, except for the $D\,^1\Pi$ state. In this case the result indicates that the calculated wavefunction and energy corresponds more to a pseudo state that is a mixture of the correct $D\,^1\Pi$ state and some Rydberg states of the same symmetry, the latter not being explicitly represented by the adopted basis set.

In order to simulate D_2 and T_2, the remaining entries of Table 5 correspond to the internuclear distance $R = 1.43a_0$. If the central molecule is surrounded by one shell of next neighbours (I', II', or III'), all excitation energies are shifted to higher values. Since the ground state is shifted by less than 0.03 eV for all three clusters, the large energy shifts of up to 2.46 eV that are found for the excitation energies are evidently due to a comparatively strong and repulsive interaction of the excited central molecule and its neighbours. This repulsive interaction is of different strength for different final states, and it depends on the cluster geometry. As one would expect from a simple confinement argument, the largest shifts are found for cluster II, where the distance between the central molecule and the closest lying atoms is smallest. However, in the case of the $B\,^1\Sigma_u^+$ and $C\,^1\Pi_u$ states the energy shifts are very similar for all three clusters, indicating that a more complex mechanism is responsible for the energy shift.

Adding the second shell of neighbour molecules leads to a further, but smaller shift of the excitation energies for most of the states. Again the $B\,^1\Sigma_u^+$ and $C\,^1\Pi_u$ states are exceptions, since they are nearly unaffected by the second shell. In some cases the excitation energy is in fact slightly decreased. The two states are accompanied by the $I\,^1\Pi_g$ state that also does not show a further increase of the excitation energy when adding the second shell. The (small) decrease in excitation energy again indicates that a more complicated interaction than pure electron-electron repulsion or Pauli blocking takes place, this effect being however evidently smaller than the repulsive interaction. It may also be noted that the ground state energy is nearly unaffected by adding the second shell of surrounding molecules, as one would expect.

In principle, more and more shells of surrounding molecules would have to be added until complete convergence is reached. For reasons of computation time, the present calculation was however limited to two shells, since it seems evident that the main features of the solid surrounding should be visible from the results obtained with these two shells. Another question is of course, how much the present results depend on the accuracy of the wavefunctions used in the description of the surrounding molecules. In order to allow an estimate of this effect, in Table 5 the results obtained with a much poorer basis set than the one adopted in the remaining calculations is also given. In this case, denoted by $\tilde{I}''$, a so-called STO-3G basis set is adopted for the surrounding molecules. This basis set contains only a single s-type basis function that is formed by three (contracted) Gaussians and yields a Hartree-Fock ground state energy of -30.39 eV. As can be seen from Table 5, the results are very similar to the corresponding ones obtained with the much better quality basis set adopted in the remaining calculations. However, the predicted energy shifts are consistently larger, if calculated with the poorer basis. This result confirms that the overall results presented in this work should be rather converged with respect to the

Table 5. Excitation energies $E_{\rm exc}$ (in eV) and oscillator strength values f (in parenthesis) for an H_2 molecule that is either free or surrounded by different H_2 clusters. (See text for a definition of the symbols denoting the different clusters.)

System	$B\,^1\Sigma_u^+$	$E,F\,^1\Sigma_g^+$	$C\,^1\Pi_u$	$B'\,^1\Sigma_u^+$	$H\,^1\Sigma_g^+$	$I\,^1\Pi_g$	$D\,^1\Pi_u$
H_2 ($R=1.40a_0$)	12.75 [21]	13.13 [22]	13.22 [21]	14.85 [21]	14.60 [22]*	14.92 [23]	14.99 [21]
this work	12.71	13.16	13.24	14.99	14.61*	14.96	16.07
H_2 ($R=1.43$)	12.57	13.06	13.13	14.86	14.87	14.84	15.95
	(0.309)		(0.168)	(0.090)			(0.194)
I'(1.43/9.65)	13.37	15.15	14.44	15.27	15.65	16.34	16.74
	(0.450)		(0.338)	(0.002)			(0.024)
II'(1.43/9.65)	13.34	15.52	14.47	15.61	15.86	16.71	16.99
	(0.451)		(0.347)	(0.002)			(0.016)
III'(1.43/9.65)	13.33	15.06	14.44	15.17	15.52	16.24	16.56
	(0.446)		(0.332)	(0.001)			(0.030)
I"(1.43/9.65)	13.35	15.54	14.46	15.84	16.58	16.27	17.59
	(0.448)		(0.344)	(0.005)			(0.019)
II"(1.43/9.65)	13.33	15.71	14.48	16.23	16.97	16.71	17.84
	(0.450)		(0.350)	(0.006)			(0.014)
III"(1.43/9.65)	13.31	15.52	14.46	15.72	16.38	16.17	17.40
	(0.444)		(0.341)	(0.004)			(0.023)
I"(1.43/9.25)	13.49	16.07	14.65	15.76	16.78	16.12	17.51
	(0.463)		(0.362)	(0.008)			(0.007)
I"(1.43/9.45)	13.42	15.81	14.55	15.80	16.67	16.20	17.55
	(0.455)		(0.353)	(0.007)			(0.012)
I"(1.43/9.85)	13.28	15.30	14.37	15.88	16.49	16.34	17.62
	(0.440)		(0.335)	(0.004)			(0.027)
I"(1.43/10.05)	13.22	15.07	14.28	15.93	16.41	16.40	17.64
	(0.432)		(0.327)	(0.003)			(0.036)
I"(1.43/12.00)	12.82	13.73	13.68	16.22	15.77	16.25	17.35
	(0.371)		(0.257)	(0.008)			(0.114)
I"(1.43/15.00)	12.62	13.17	13.28	15.71	15.27	15.50	16.48
	(0.327)		(0.199)	(0.103)			(0.171)
I"(1.43/20.00)	12.58	13.06	13.14	15.00	14.94	14.93	16.00
	(0.310)		(0.171)	(0.099)			(0.192)
I"(1.43/30.00)	12.57	13.06	13.13	14.86	14.87	14.84	15.95
	(0.309)		(0.168)	(0.090)			(0.194)
$\tilde{I}''$(1.43/9.65)	13.40	15.69	14.51	15.89	16.73	16.41	17.78
	(0.449)		(0.345)	(0.005)			(0.017)

* The values are given for the internuclear distance $R=1.50a_0$.

basis set used for describing the surrounding molecules. However, it indicates also that the shape of the surrounding wavefunctions is important, and a very simple model that *e.g.* assumes the environment to consist out of non-interacting hydrogen atoms will only give a very crude estimate of the solid state effects.

Since the exact molecular geometry of the quench condensed D_2 films is not known and since the hydrogen molecules are even in the solid not fixed in space, it was felt important to investigate the influence that the average distance between the central molecule and its surrounding has on the results[5]. This was done by calculating the excitation energies as a function of the length of the unit cell parameter a. In Table 5 the results are given for cluster I" as an representative example. From the results it may be concluded that an error in the average distance will affect the numbers itself, but the basic effect is independent of the exact value of the average intermolecular distance. In most cases it is observed that a decrease

[5] It may be noted that for the different hydrogen isotopes (assuming a closely-packed *fcc* crystal) the unit cell parameters a are $10.12a_0$ (H_2), $9.65a_0$ (D_2), and $9.45a_0$ (T_2), respectively.

Table 6. Averaged excitation energies $\bar{E}_{\rm exc}$ and averaged oscillator strength values $\bar{f}$ of an H_2 molecule in a cluster surrounding. Also the shifts of the excitation energy ($\Delta E_{\rm exc}$) and the oscillator strength (Δf) compared to their values for a free H_2 molecule are listed (all energies are given in eV).

	$B\,^1\Sigma_u^+$	$E, F\,^1\Sigma_g^+$	$C\,^1\Pi_u$	$B'\,^1\Sigma_u^+$	$H\,^1\Sigma_g^+$	$I\,^1\Pi_g$	$D\,^1\Pi_u$
$\bar{E}_{\rm exc}$	13.33	15.59	14.47	15.93	16.64	16.38	17.61
$\Delta E_{\rm exc}$	+0.76	+2.53	+1.34	+1.07	+1.77	+1.54	+1.66
$\bar{f}$	0.447		0.345	0.005			0.019
Δf	+0.138		+0.177	−0.085			−0.175

of the intermolecular distance leads to a steady increase of the excitation energy. Again, there are however some exceptions ($B'\,^1\Sigma_u^+$, $I\,^1\Pi_g$, and $D\,^1\Pi_u$) where the excitation energy exhibits some local maximum and follows the main trend only on a large scale. For the unit cell parameter $a = 30.0a_0$ the results agree to the ones obtained for a free molecule within the number of digits given in the table.

It may be noted, that the energy range spanned by electronically excited, but bound states will decrease when going from the gas phase to the condensed one. This is due to the fact that the energy of the lowest lying excited state ($B\,^1\Sigma_u^+$) increases, while the energy of the ground state of the hydrogen molecular ion decreases (due to polarisation effects) when going from the gaseous to the solid phase. Considering the lowering of the ionisation threshold and the comparatively large energy shifts of the higher lying electronic states when going from the gaseous to the solid phase, it may be noted that these higher lying states may in fact be shifted into the electronic continuum, and thus become autoionising states due to the solid environment. This effect might lead to some structure in the ionisation spectrum, as is seemingly observed in some previous experiments.

Due to nuclear motion, one has in fact also a distribution of intramolecular distances R. The experimentally observed final state energy distribution will thus be broadened and modified by the Franck-Condon factors of the electronic ground state, even if purely vertical transitions are considered. The influence of a variation of R (of the central molecule) has thus been investigated. It turns out that the absolute values of the excitation energies will change. Some of these changes are in fact rather large due to the repulsive character of the final state potential curves. However, the shift with respect to the excitation energy of a free molecule is to a good approximation constant in between $R = 1.30$ and $1.50a_0$.

The results of the theoretical model adopted in this work are summarised in Table 6 where the average excitation energies and the shifts with respect to a free molecule are given. These results have been obtained after averaging the results obtained for clusters I", II", and III". A large energy shift (in between 0.76 and 2.53 eV) is found for all excited states that have been considered. This explains directly the energy shifts observed in the experiment. The magnitude of the shift (the average shift of the states considered is 1.52 eV) is also in quantitative agreement with the experimental results, considering the approximations adopted in the theoretical model. It may however be reminded that the present model is likely to overestimate the confinement effects.

Besides the change of the excitation energies, a second question to answer would be the one concerning the change of spectral intensities when going from the gas phase to the solid. In order to predict the spectral changes of the electron energy loss, it would be required to evaluate the inelastic cross-section for electrons scattered off the central molecule. Considering the fact that the energy of the incident electrons is of the order of 18 keV, it should be sufficient to ignore exchange contributions and to treat the problem within the first Born approximation. This would then require to evaluate the generalised oscillator strength values for every excited state as a function of the momentum transfer, and to integrate over all possible momentum transfers. In order to avoid rather time consuming calculations, but still to obtain some idea of the spectral changes, only the optical oscillator strength values f have been evaluated. For optically allowed transitions, the generalised oscillator strength density will usually have its maximum in the optical limit, so the changes in f should give some indication of the changes of the generalised oscillator strength values. This is of course not true for the optically forbidden transitions. Nevertheless, since for high incident energies the scattering processes will be dominated by small angle scattering and the generalised oscillator strength is proportional to the optical one in the limit $K \to 0$ (where K is the absolute value of the scattering vector), the optical oscillator-strength values should give some qualitative idea also for the energy loss spectrum, but will not allow a prediction of the inelastic scattering cross-section $\sigma_{\rm tot}$ itself.

In Table 5 the optical oscillator strength values f are listed for the optically allowed transitions. Evidently, the photoabsorption cross-sections (being proportional to f) for the $B\,^1\Sigma_u^+$ and the $C\,^1\Pi_u$ states change by a factor $\sim$ 1.5 and $\sim$ 2, respectively, when going from the gas phase to the solid. On the other hand, the $B'\,^1\Sigma_u^+$ and $D\,^1\Pi_u$ will have much smaller cross-section in the solid state compared to the gas phase. The influence of adding the second shell of surrounding molecules is quite small, except for the $D\,^1\Pi_u$ state. A change of the intermolecular distances has a similar effect on the cross-sections as it had for the energies. Averaging again over the results obtained for the clusters I", II", and III" gives our final

estimate listed in Table 6. In contrast to the energy shift, the shifts of the oscillator strength values are partly positive, partly negative. This has to be the case, since within the presently adopted model the Thomas-Kuhn sum rule should be fulfilled, *i.e.* the sum over all values of f should be equal to 2 (the number of *active* electrons). Although four values of f are not very representative, the results seem again to support the confinement idea, since the higher lying and spatially more extended states loose excitation probability which in turn is transfered to the lower lying, spatially less extended states. Since the shifts for the explicitly considered states add up to a positive number, the sum rule predicts that the even higher lying excited states (including the electronic continuum) will (in total) loose transition probability.

Due to the broadening by rovibrational motion, the transitions to higher lying electronic bound states cannot easily be distinguished from ionisation in simple photoabsorption or energy loss spectra, especially if not very high resolution is achieved. It is very likely, that in a typical photoabsorption spectrum on gaseous hydrogen only the $B\,^1\Sigma_u^+$ and the $C\,^1\Pi_u$ (in energy loss spectra also the $E, F\,^1\Sigma_g^+$) states may clearly be recognisable as electronic excitations (and should correspond to the peak of the energy loss function (8) at ϵ_1 in Sect. 2). According to the present theoretical model these states will gain transition probability when going to the solid phase, but both the $E, F\,^1\Sigma_g^+$ and the $C\,^1\Pi_u$ will be shifted to rather high energies. Considering additionally that the ionisation threshold itself is shifted to lower energies in the solid compared to the gas, it is likely that basically only the $B\,^1\Sigma_u^+$ may contribute to what is designated as excitation peak, while all others merge into the electronic continuum. This fact (together with the shift of excited states over the ionisation threshold) would explain the enhanced relative ionisation observed in the experiments on solid D_2 (Sect. 3) compared to the one found for gaseous T_2 (Sect. 2) as is visible from Figure 7. Of course, more elaborate calculations and experiments with higher resolution would be required in order to allow a direct comparison between theoretical and the experimental energy loss spectrum.

In conclusion, the present theoretical model predicts that the edge of photon absorption or energy loss will be shifted to larger excitation energies (by about 0.76 eV). The mean excitation energy of the bound states considered will even be shifted by about 1.52 eV. At least in the case of photoabsorption, but most likely also in the energy loss spectrum, the energetically low lying states will gain transition probability, while the higher lying states (including the electronic continuum) loose transition probability. These results agrees well with the experimental observation that the excitation spectrum is different for gaseous and solid hydrogen and exhibits a higher threshold, although the ground state molecules in the solid behave nearly as they would be free even in the condensed phase. The results also confirm that this effect is basically due to a kind of confinement of the wavefunctions of the excited molecule by the surrounding. This spatial limitation caused by electrostatic repulsion and Pauli blocking will energetically disfavour spatially extended states of the central molecule. While this seems to be the basic effect, the present investigation indicates also, that there exist some (though minor) deviations from this simplified model that should be due to the more complicated quantum mechanical interaction between the central molecule and its surrounding. A model aiming for a fully quantitative description will thus have to include those effects, which is only partly done in the present model where the surrounding has been described within a static approximation. In addition, the computation has to include a larger range of excitation energies (including the non-resonant ionisation) and should be extended beyond the optical limit ($K \to 0$), if theoretical predictions regarding the total inelastic electron impact cross-section $\sigma_{\rm tot}$ should become possible.

5 Conclusion

Measurements of the energy loss of fast electrons at an energy of 18 keV have been performed on molecules of hydrogen isotopes, gaseous T_2 and frozen D_2.

In the case of gaseous T_2 the total inelastic cross-section, integrated over all scattering angles and energy losses has been found to be $\sigma_{\rm tot,\ gaseous} = (3.40 \pm 0.07) \times 10^{-18}$ cm^2 in agreement with theory [9]. The mean energy loss in gaseous T_2 has been measured to be $\overline{\varepsilon}_{\rm gaseous} = (29.9 \pm 1.0)$ eV. The product $\sigma_{\rm tot}\overline{\varepsilon}$ is in agreement with established stopping power values [12]. The shape of the energy loss spectrum is well described by a Gaussian centered at 12.6 eV, which is smoothly connected to an appropriate tail function. The peak position coincides with the first electronic excitation band of molecular hydrogen.

In contrast to the overall agreement of our results with the expectations for gaseous T_2 the energy loss of 18 keV electrons in quench condensed D_2 exhibits significant differences. The total inelastic cross-section has been found to be $\sigma_{\rm tot,\ solid} = (2.98 \pm 0.16) \times 10^{-18}$ cm^2 which is reduced by 13% compared to the value for gaseous T_2. The average energy loss in quench condensed D_2, $\overline{\varepsilon}_{\rm solid} = (34.4 \pm 3.0)$ eV, is 4.5 eV above the corresponding value of gaseous T_2. Using a similar parametrisation of the energy loss function as for gaseous T_2 gives a significant shift in the peak position, $\varepsilon_{1,\ \rm solid} = 14.1^{+0.7}_{-0.6}$ eV, towards higher energy losses. All these effects may be interpreted in terms of changes in the final states spectrum.

To this end CI calculations within a molecular cluster have been performed. They show indeed that the excited states of the central molecule are shifted up by an average of about 1.52 eV, whereas the molecular ground state remains basically unaffected. These calculations also indicate a change of the individual transition probabilities when going from the gaseous to the solid state.

By the help of these results we are now in the position to calculate safely the energy loss in gaseous or solid T_2 sources, whose β decay spectrum serves for the determination of the rest mass of the neutrino to the present sensitivity limit of 2 eV/c^2 [7,8].

However, there remain residual uncertainties with respect to the detailed shape of the energy loss spectrum.

This is inherent to our experimental method of measuring integral energy loss spectra by MAC-E-filters. The planned new generation of tritium β spectrometers of this type [24,25] will overcome this problem by having the option of a non-integrating mode.

We would like to thank P. Leiderer for helpful discussions. This work was partially supported by grant INTAS-RFBR 95-0819 and by the Deutsche Forschungsgemeinschaft under contract Ot33/13. We would like to thank the ISOLDE collaboration/CERN for kindly providing the ^{83}Rb source. One of the authors (V.L.) is indebted to the Alexander-v-Humboldt Foundation for the Research grant.

References

1. J. Geiger, Z. Phys. **181**, 413 (1964).
2. R. Ulsh *et al.*, J. Chem. Phys. **60**, 103 (1973).
3. L. Schmidt, Phys. Lett. A **36**, 87 (1971).
4. M.W. Ruckman, J.F. Moore, Phys. Rev. B **47**, 8407 (1993).
5. A. Gedanken *et al.*, J. Chem. Phys. **59**, 2752 (1973).
6. K. Inoue *et al.*, Solid State Commun. **30**, 627 (1979).
7. V.M. Lobashev *et al.*, Phys. Lett. B **460**, 227 (1999), and references therein.
8. Ch. Weinheimer *et al.*, Phys. Lett. B **460**, 219 (1999), and references therein.
9. J.W. Liu, Phys. Rev. A **7**, 1 (1973).
10. Ch. Weinheimer *et al.*, Phys. Lett. B **300**, 210 (1993).
11. B.L. Schram *et al.*, Physica **31**, 1 (1965).
12. L. Pages *et al.*, Atomic Data **4**, 1 (1972).
13. CERN Library Long Writeup D506, vers. 92.1 of March 1992
14. V.B. Berestetskii *et al.*, *Landau and Lifshitz: Course of Theoretical Physics/Quantum Electrodynamics*, 2nd edn. (Pergamon Press, New York, 1982).
15. A. Picard *et al.*, Nucl. Instrum. Meth. B **63**, 345 (1992).
16. A. Picard *et al.*, Z. Phys. A **342**, 71 (1992).
17. M. Przyrembel, doctoral thesis, Mainz university, 1995.
18. The mother isotop Rb-83 was kindly provided by the ISOLDE collaboration/CERN.
19. I.F. Silvera, Rev. Mod. Phys. **52**, 393 (1980).
20. M.W. Schmidt *et al.*, J. Comp. Chem. **14**, 1347 (1993).
21. L. Wolniewicz, K. Dressler, J. Chem. Phys. **88**, 3861 (1988).
22. J.W. Liu, S. Hagstrom, Phys. Rev. A **48**, 166 (1993).
23. W. Kołos, J. Rychlewski, J. Mol. Spectrosc. **66**, 428 (1977).
24. J. Bonn *et al.*, Nucl. Instrum. Meth. A **421**, 256 (1999).
25. V.M. Lobashev, Prog. Part. Nucl. Phys. **40**, 337 (1998).